Journal of Solid State Chemistry **153,** 263–269 (2000)
doi:10.1006/jssc.2000.8753, available online at http://www.idealibrary.com on IDEAL®

Spin Dimer Analysis of the Spin Exchange Interactions of the Vanadium Oxides AV_4O_9 (A = Ca, Sr, Cs_2, $NH_2(CH_2)_4NH_2$)

H.-J. Koo and M.-H. Whangbo[1]

Department of Chemistry, North Carolina State University, Raleigh, North Carolina 27695-8204

Received February 22, 2000; in revised form April 17, 2000; accepted April 20, 2000; published online July 7, 2000

The spin exchange interactions of the vanadium oxides AV_4O_9 (A = Ca, Sr, Cs_2, and $NH_2(CH_2)_4NH_2$) were examined by calculating the spin orbital interaction energies of their spin dimers based on the extended Hückel method. The temperature T_{max} at which the magnetic susceptibility maximum occurs in AV_4O_9 (A = Ca, Sr, Cs_2, and $NH_2(CH_2)_4NH_2$) shows a wide variation (from 30 to 600 K) and increases in the order $[NH_2(CH_2)_4NH_2]V_4O_9 < CaV_4O_9 < Cs_2V_4O_9$. The susceptibility at T_{max} increases in the opposite order, and the room temperature susceptibility of $[NH_2(CH_2)_4NH_2]V_4O_9$ is about twice as high as the maximum susceptibility of CaV_4O_9. These observations were examined by estimating the magnetic excitation energies of the strongly interacting spin units of AV_4O_9. © 2000 Academic Press

1. INTRODUCTION

In the vanadium oxides AV_4O_9 (A = Ca, Sr, Cs_2, and $NH_2(CH_2)_4NH_2$), the $(V_4O_9)^{2-}$ layers made of VO_5 square pyramids are separated by the A^{2+} cations (1–4). (Here, the organic dication $A^{2+} = [NH_2(CH_2)_4NH_2]^{2+}$ refers to the doubly protonated species of piperazine, $HN(CH_2)_4NH$, a six-membered-ring cyclic diamine.) The oxidation state of each vanadium is 4+, so each $(VO_5)^{6-}$ square pyramid constitutes a spin monomer (i.e., a structural unit containing an unpaired spin). For different cations A^{2+} the $V_4O_9^{2-}$ layers of AV_4O_9 differ in the way the VO_5 square pyramids are condensed, as shown in Figs. 1a–1c for $[NH_2(CH_2)_4NH_2]V_4O_9$, AV_4O_9 (A = Ca and Sr) and $Cs_2V_4O_9$, respectively, where each small square with solid (dotted) diagonal lines represents a VO_5 square pyramid having the apical oxygen atom above (below) the basal plane, and each large square consisting of four small squares represents a plaquette (PLQ). The magnetic susceptibilities of $[NH_2(CH_2)_4NH_2]V_4O_9$, AV_4O_9 (A = Ca and Sr) and $Cs_2V_4O_9$ show a broad maximum at $T_{max} \approx 30$, 100, and 600, as depicted Figs. 2a–2c, respectively (2–5). The susceptibility plots exhibit two striking features: (a) The T_{max} value shows a wide variation and increases in the order $[NH_2(CH_2)_4NH_2]V_4O_9 < CaV_4O_9 < Cs_2V_4O_9$. (b) The susceptibility at T_{max} (i.e., χ_m) increases in the opposite order, i.e., $[NH_2(CH_2)_4NH_2]V_4O_9 > CaV_4O_9 > Cs_2V_4O_9$. The room temperature susceptibility of $[NH_2(CH_2)_4NH_2]V_4O_9$ is nearly twice as high as the χ_m value of CaV_4O_9. The latter indicates the presence of another excitation thermally accessible. Zhang *et al.* (4) explained these observations in terms of the spin orbital interaction energies calculated for the spin dimers (i.e., structural units containing two adjacent spins) of AV_4O_9 using extended Hückel molecular orbital calculations (6). However, this study considered the spin exchange interactions of edge-sharing spin dimers but neglected those of corner-sharing spin dimers. The analyses of the neutron inelastic scattering data and the magnetic susceptibility of CaV_4O_9 (7, 8) revealed that the strongest spin exchange interaction in CaV_4O_9 occurs through a corner-sharing spin dimer and so did the first principles electronic structure calculations for CaV_4O_9 (8, 9). In addition, according to our studies (10–13) of other magnetic solids of vanadium and copper, the trends in the spin exchange parameters are reproduced in terms of spin orbital interaction energies if the latter are calculated by using double-ζ Slater-type orbitals (DZ-STOs) (14) for both the transition metal d and the ligand s/p orbitals. In the study of Zhang *et al.* (4), the V 3d orbitals were represented by DZ-STOs, but the oxygen 2s/2p orbitals by single-ζ Slater-type orbitals (SZ-STOs). In the present work we re-examine the spin exchange interactions of AV_4O_9 (A = Ca, Sr, Cs_2, and $NH_2(CH_2)_4NH_2$) by calculating the spin orbital interaction energies of their corner- and edge-sharing spin dimers using DZ-STOs for both the vanadium 3d and the oxygen 2s/2p orbitals. Based on these calculations, we identify the strongly interacting spin units (SISUs) of the AV_4O_9 systems, set up the spin Hamiltonian appropriate for the SISUs, and determine the magnetic excitation energies associated with the Hamiltonians. Based on these energies, we discuss why the T_{max} values of AV_4O_9 have a wide variation and why the second excitation energy of $[NH_2(CH_2)_4NH_2]V_4O_9$ is thermally accessible.

[1]To whom correspondence should be addressed.

0022-4596/00 $35.00
Copyright © 2000 by Academic Press
All rights of reproduction in any form reserved.

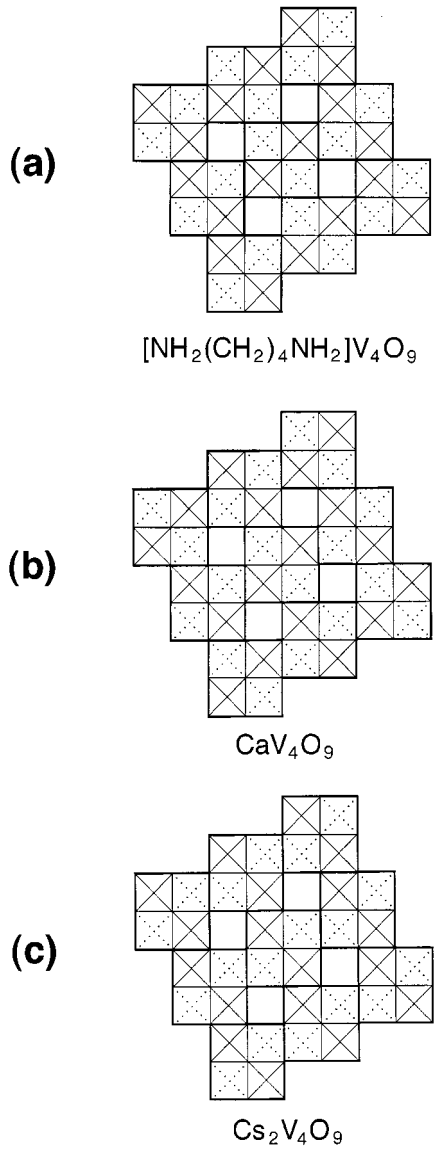

FIG. 1. Condensation patterns of the $(V_4O_9)^{2-}$ layers of (a) $[NH_2(CH_2)_4NH_2]V_4O_9$, (b) CaV_4O_9, and (c) $Cs_2V_4O_9$. Each small square with solid (dotted) diagonal lines represents a VO_5 square pyramid having the apical oxygen atom above (below) the basal plane, and the large square made up of four small squares represents a plaquette (PLQ).

2. SPIN DIMERS AND SPIN ORBITAL INTERACTION ENERGIES

The edge- and corner-sharing spin dimers of AV_4O_9 (A = Ca, Sr, Cs_2, and $NH_2(CH_2)_4NH_2$) are the $(V_2O_8)^{8-}$ and $(V_2O_9)^{10-}$ clusters (Figs. 3a and 3b, respectively). All possible nearest neighbor edge- and corner-sharing spin dimers of AV_4O_9 are defined in the schematic diagram of Fig. 3c, which shows the arrangement of five adjacent PLQs. The numbers 1–12 in Fig. 3c indicate all unique intra- and inter-PLQ interactions that occur through edge- and corner-sharing spin dimers. These interactions are all different in $[NH_2(CH_2)_4NH_2]V_4O_9$, while the interactions 1–4, 5 and 6, 7 and 8, and 9–12 are each equivalent in AV_4O_9 for A = Ca, Sr, and Cs_2. The nearest neighbor spin exchange parameter J of a spin dimer is related to the energy difference ΔE between the triplet and singlet states of the corresponding spin dimer, i.e., $J = \Delta E = {}^1E - {}^3E$ (15–17). In general, J is written as $J = J_F + J_{AF}$, where the ferromagnetic term J_F favors the triplet state (i.e., $J_F > 0$), while the

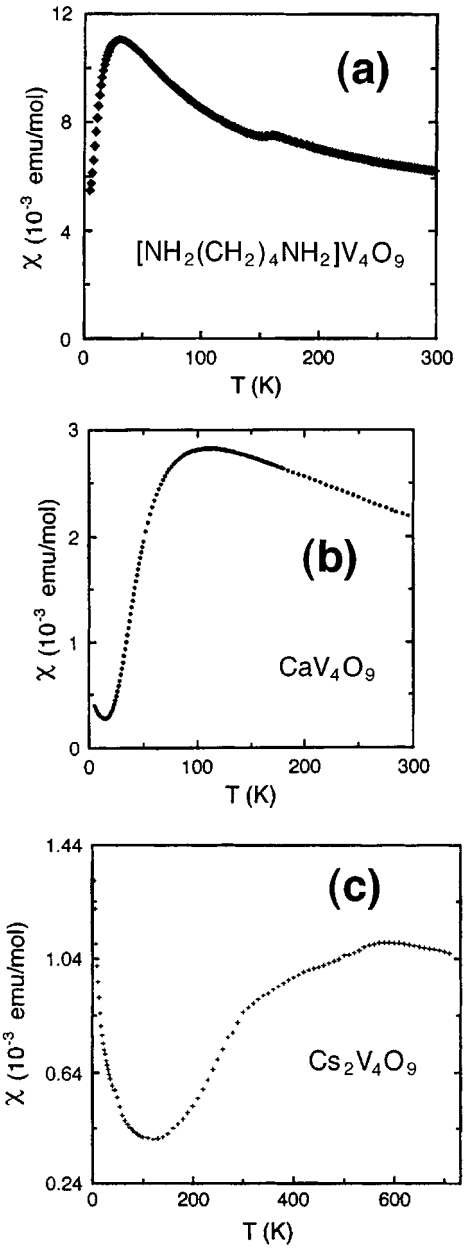

FIG. 2. Magnetic susceptibilities of (a) $[NH_2(CH_2)_4NH_2]V_4O_9$, (b) CaV_4O_9, and (c) $Cs_2V_4O_9$ as a function of temperature (modified from Ref. (4)).

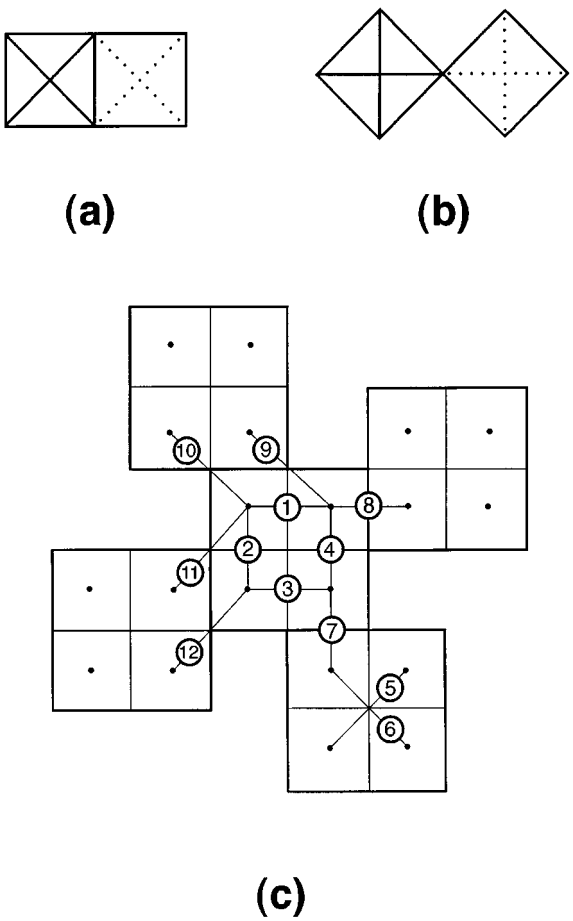

FIG. 3. Schematic projection views of (a) the edge-sharing spin dimer $(V_2O_8)^{8-}$, (b) the corner-sharing spin dimer $(V_2O_9)^{10-}$, and (c) the arrangement of five PLQs. The numbers in (c) enumerate the unique spin exchange interactions of V_4O_9.

antiferromagnetic term J_{AF} favors the singlet state (i.e., $J_{AF} < 0$). Qualitative trends in the J parameters of an extended magnetic solid are explained in terms of spin orbital interaction energies calculated for the corresponding spin dimers using extended Hückel molecular orbital calculations (10–13). For the interaction between two equivalent spins, $|J_{AF}|$ increases with increasing Δe, where Δe is the energy separation between the highest two singly occupied energy levels of a spin dimer (Fig. 4a). For the interaction between two nonequivalent spins, $|J_{AF}|$ increases with the net change in orbital energy, $(\Delta e - \Delta e^0)$ (Fig. 4b) (12, 17). For antiferromagnetic systems, the qualitative trend in the $|J|$ parameters can be understood by studying that of the corresponding $(\Delta e - \Delta e^0)$ values (for the interaction between two equivalent spins, $\Delta e^0 = 0$). The parameters of the atomic orbitals used in our calculations are listed in Table 1 (18).

TABLE 1

Exponents (ζ_i and $\zeta_{i'}$) and Valence Shell Ionization Potentials (H_{ii}) of Slater-Type Orbitals (χ_i) Used for Extended Hückel Molecular Orbital Calculations[a]

Atom	χ_i	H_{ii} (eV)	ζ_i	c_1[b]	$\zeta_{i'}$	c_2[b]
V	4*s*	− 8.81	1.697	1.0		
V	4*p*	− 5.52	1.260	1.0		
V	3*d*	− 11.0	5.052	0.3738	2.173	0.7456
O[c]	2*s*	− 32.3	2.688	0.7076	1.675	0.3745
O[c]	2*p*	− 14.8	3.694	0.3322	1.659	0.7448
O[d]	2*s*	− 32.3	2.275	1.0		
O[d]	2*p*	− 14.8	2.275	1.0		

[a] H_{ii}'s are the diagonal matrix elements $\langle\chi_i|H^{\text{eff}}|\chi_i\rangle$, where H^{eff} is the effective Hamiltonian. In our calculations of the off-diagonal matrix elements $H_{ij} = \langle\chi_i|H^{\text{eff}}|\chi_j\rangle$, the weighted formula was used. See J. Ammeter, H.-B. Bürgi, J. Thibeault, and R. Hoffmann, *J. Am. Chem. Soc.* **100,** 3686 (1978).

[b] Contraction coefficients used in the double-ζ Slater-type orbital.

[c] Double-ζ Slater-type orbital.

[d] Single-ζ Slater-type orbital.

3. RESULTS AND DISCUSSION

The spin exchange parameters of CaV_4O_9 for the interactions 1, 5, 7, and 9 are known from the neutron inelastic scattering and magnetic susceptibility studies (5, 8) and from first-principles electronic structure calculations (8, 9), as summarized in Table 2. The $(\Delta e - \Delta e^0)$ values of the spin dimers 1, 5, 7, and 9 calculated by using the DZ-STO's for both the V 3*d* and O 2*s*/2*p* orbitals (referred to as the DZ/DZ calculation) are also listed in Table 2. For comparison, the $(\Delta e - \Delta e^0)$ values were also calculated using the DZ-STOs for the V 3*d* and the SZ-STOs for the O 2*s*/2*p* orbitals (referred to as the DZ/SZ calculation). In general, the spin exchange parameters derived from experiments and first-principles calculations are in good agreement. The trend in the relative magnitudes of these spin exchange

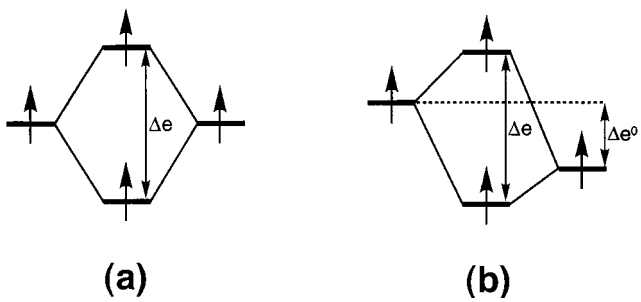

FIG. 4. Interaction between spin monomers leading to the two singly filled energy levels of a spin dimer: (a) between equivalent spin monomers and (b) between nonequivalent spin monomers.

TABLE 2
Experimental and Calculated Spin Exchange Parameters and Spin Orbital Interaction Energies of CaV_4O_9 (in meV Units)

		Corner-sharing		Edge-sharing	
		Inter PLQ	Intra PLQ	Inter PLQ	Intra PLQ
$-J_{exp}$	Neutron scattering[a]	14.73	1.25	5.76	5.76
	Magnetic susceptibility[b]	14.2	3.7	9.6	9.3
$-J_{calc}$	Calculations (LDA + U)[c]	12.75	7.84	5.34	7.67
	Calculations (LSDA)[b]	23.8	6.5	1.1	8.9
	Calculations (SCAD)[b]	19.3	3.9	12.5	9.7
$(\Delta e - \Delta e^0)$	DZ/DZ[d]	193	90	72	76
	DZ/SZ[e]	196	141	298	307

[a]Ref. (5).
[b]Ref. (8).
[c]Ref. (9).
[d]Double-ζ Slater-type orbitals for both the V 3*d* and the O 2*s*/2*p* orbitals.
[e]Double-ζ Slater-type orbitals for the V 3*d* orbital and the single-ζ orbitals for O 2*s*/2*p* orbitals.

parameters is very well reproduced by the $(\Delta e - \Delta e^0)$ values obtained from the DZ/DZ calculation, but not by those obtained from the DZ/SZ calculations. This is consistent with the conclusion of our studies on other magnetic solids (10–13). Thus, it is strongly suggested that in studying the qualitative trend in the spin exchange parameters of a magnetic solid of a transition metal element, one calculates the spin orbital interaction energies of spin dimers by using DZ-STOs for both the transition metal *d* and ligand *s*/*p* orbitals.

Table 3 summarizes the $(\Delta e - \Delta e^0)$ values of AV_4O_9 (A = Ca, Sr, Cs_2, and $NH_2(CH_2)_4NH_2$) obtained by the DZ/DZ calculations. The small differences between the spin orbital interaction energies in the same column are not significant, so we will focus on the qualitative trends in these energies. Rigorously speaking, the spin orbital interaction energies of the corner- and edge-sharing spin dimers can be compared only under the assumption that the two-electron Coulomb and exchange interactions are roughly identical in the two cases (15). This assumption is well justified, as can be seen from Table 2; the spin orbital interaction energies calculated for CaV_4O_9 quite well reproduce the trend in the relative magnitudes of the spin exchange parameters derived from experiments and first-principles calculations.

The $(\Delta e - \Delta e^0)$ values of Table 3 indicate that the strongest spin exchange interactions form dumbbell SISUs in $Cs_2V_4O_9$ and square SISUs in AV_4O_9 (A = Ca and Sr), as shown by solid lines in Figs. 5a and 5b, respectively. The interactions between SISUs, shown by dotted lines, form a two-dimensional (2D) network. In $[NH_2(CH_2)_4NH_2]V_4O_9$ the two strongest spin exchange interactions form zigzag SISUs, as shown by the solid lines in Fig. 5c, where the interactions between the zigzag SISUs form one-dimensional (1D) chains. To a first approximation, the magnetic excitation energies of AV_4O_9 (A = Ca, Sr, Cs_2, and $NH_2(CH_2)_4NH_2$) are largely determined by the energy gap between the ground and the first excited states of their SISUs. In the following we estimate the relative magnitudes

TABLE 3
Spin Orbital Interaction Energies $(\Delta e - \Delta e^0)$ (in meV) Calculated for the Various Spin Dimers of AV_4O_9

	Corner-sharing interaction				Edge-sharing interaction			
A	Inter PLQ[a]		Intra PLQ[a]		Inter PLQ[a]		Intra PLQ[a]	
$NH_2(CH_2)_4NH_2$	224	(9)	73	(5)	446	(7)	7	(1)
	221	(10)	49	(6)	57	(8)	0	(2)
	136	(11)					5	(3)
	171	(12)					0	(4)
α-Cs_2	193	(9–12)	45	(5, 6)	318	(7, 8)	54	(1–4)
β-Cs_2	225	(9–12)	48	(5, 6)	327	(7, 8)	50	(1–4)
Ca	193	(9–12)	90	(5, 6)	72	(7, 8)	76	(1–4)
Sr	191	(9–12)	91	(5, 6)	70	(7, 8)	72	(1–4)

[a]The numbers in parentheses refer to the types of interactions defined in Fig. 3c.

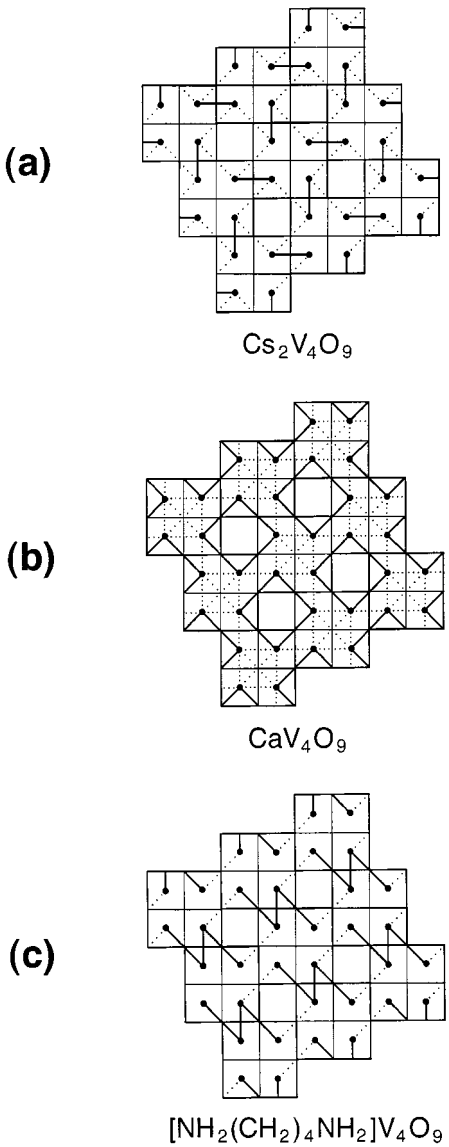

FIG. 5. Simplified representation of spin exchange interactions in (a) $Cs_2V_4O_9$, (b) CaV_4O_9, and (c) $[NH_2(CH_2)_4NH_2]V_4O_9$. The solid lines indicate the SISUs, and the dotted lines represent the weaker interactions between the SISUs.

of these energies by setting up spin Hamiltonians for the SISUs.

The spin exchange parameters appropriate for the dumbbell, square, and zigzag SISUs are shown in Figs. 6a–8a, respectively. The spin Hamiltonian and the energy of the dumbbell SISU are given by (19)

$$\hat{H}_1 = -J_1\vec{S}_1\cdot\vec{S}_2,$$

$$E_1 = -J_1S(S+1)/2,$$

where $S = 0, 1$. Thus, the excitation energy is given by $|J_1|$ (Fig. 6b). The spin Hamiltonian and the energy of the square SISU are written as (4)

$$\hat{H}_2 = -J_2(\vec{S}_1\cdot\vec{S}_2 + \vec{S}_2\cdot\vec{S}_3 + \vec{S}_3\cdot\vec{S}_4 + \vec{S}_4\cdot\vec{S}_1),$$

$$E_2 = -J_2(S(S+1) - S_a(S_a+1) - S_b(S_b+1))/2,$$

where $S = 0, 1, 2$, and $S_a, S_b = 0, 1$. The S value depends on the spin arrangement of the four sites 1–4, S_a value on that of the sites 1 and 3, and the S_b value on that of the sites 2 and 4. Thus, the first two excitation energies of the square spin unit are given by $2|J_2|$ and $3|J_2|$ (Fig. 7b). The spin Hamiltonian and the energy of the zigzag SISU are given by

$$\hat{H}_3 = -J_3\vec{S}_2\cdot\vec{S}_3 - J_4(\vec{S}_1\cdot\vec{S}_2 + \vec{S}_3\cdot\vec{S}_4),$$

$$E_3 = -J_4(S(S+1) - S_a(S_a+1) - S_b(S_b+1) - S_c(S_c+1))/2 + (J_4 - J_3)S_d(S_d+1)/2,$$

where $S = 0, 1, 2$, and $S_a, S_b, S_c, S_d = 0, 1$. The S value is determined by the spin arrangement of the four sites 1–4, the S_a value by that of the sites 1 and 3, the S_b value by that of the sites 1 and 4, the S_c value by that of the sites 2 and 4, and the S_d value by that of the sites 2 and 3. Since the magnitude of J_3 is larger than that of J_4 (see below), the first two excitation energies of the zigzag four-spin unit are given by $|J_4|$ and $2|J_4|$ (Fig. 8b).

The spin exchange parameter $|J|$ of an antiferromagnetic interaction scales with the square of the spin orbital interaction energy (15). Thus, it is estimated from the $(\Delta e - \Delta e^0)$ values of Table 3 that $J_1 \approx 2.1J_4$, $J_2 \approx 0.75J_4$, and $J_3 \approx 4.0J_4$. Consequently, the first excitation energies of $[NH_2(CH_2)_4NH_2]V_4O_9$, CaV_4O_9, and $Cs_2V_4O_9$ are approximately given by $|J_4|$, $1.5|J_4|$ and $2.1|J_4|$, respectively. This trend is consistent with the fact that the T_{max} values increase in the order $[NH_2(CH_2)_4NH_2]V_4O_9 < CaV_4O_9 < Cs_2V_4O_9$. The magnetic susceptibility of $[NH_2(CH_2)_4NH_2]V_4O_9$ in the temperature region above 30 K decreases slowly with increasing temperature, thereby suggesting that the second excited state of

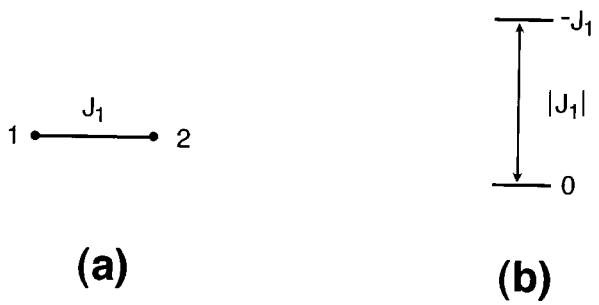

FIG. 6. (a) Spin exchange parameters and (b) excitation energies associated with the dumbbell SISU of $Cs_2V_4O_9$.

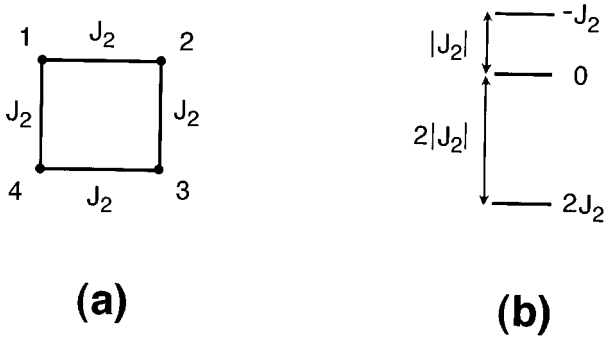

FIG. 7. (a) Spin exchange parameters and (b) excitation energies associated with the square SISU of CaV_4O_9.

$[NH_2(CH_2)_4NH_2]V_4O_9$ is thermally accessible. This is explained by the fact that the second excitation energy of $[NH_2(CH_2)_4NH_2]V_4O_9$, $2|J_4|$, lies in between the first excitation energies of CaV_4O_9 and $Cs_2V_4O_9$. The ground, first excited, and second excited states of the zigzag SISU of $[NH_2(CH_2)_4NH_2]V_4O_9$ have the spin arrangements depicted in Figs. 9a–9c, respectively.

4. CONCLUDING REMARKS

The present work shows that the trend in the spin exchange parameters of a magnetic solid of a transition metal element can be explained in terms of the spin orbital interaction energies of spin dimers calculated by using DZ-STOs for both the transition metal d and ligand s/p orbitals. The wide variation in the T_{max} values of AV_4O_9 (A = Ca, Sr, Cs_2, and $NH_2(CH_2)_4NH_2$) is well explained in terms of the first excitation energies associated with the spin Hamiltonians for their SISUs. Compared with the χ_m value of CaV_4O_9, the room-temperature magnetic susceptibility of $[NH_2(CH_2)_4NH_2]V_4O_9$ is considerably high because its second excitation energy is thermally accessible.

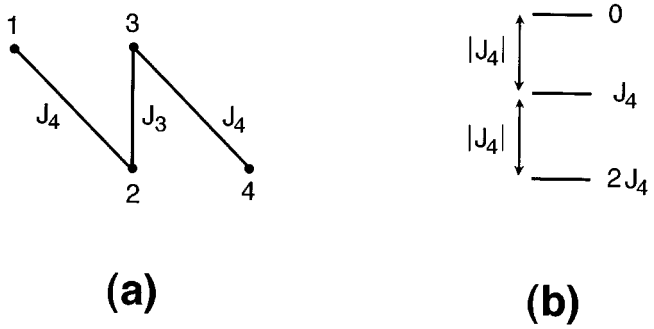

FIG. 8. (a) Spin exchange parameters and (b) excitation energies associated with the zigzag SISU of $[NH_2(CH_2)_4NH_2]V_4O_9$.

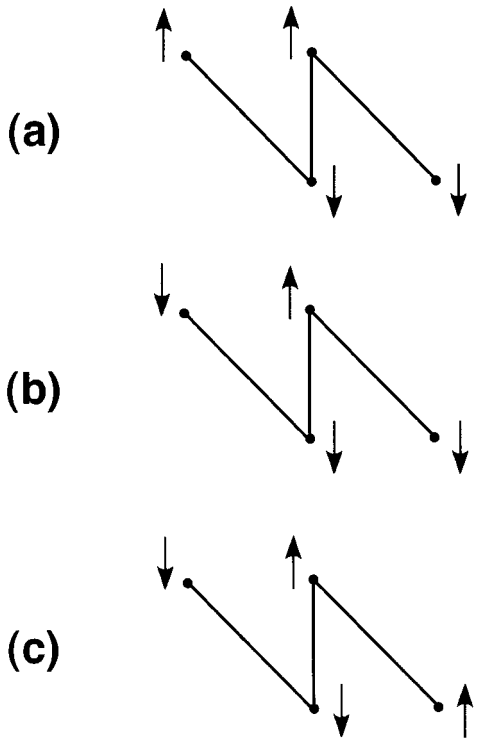

FIG. 9. Spin arrangements of (a) the ground, (b) the excited and (c) the second excited states of the zigzag SISU of $[NH_2(CH_2)_4NH_2]V_4O_9$.

ACKNOWLEDGMENT

Work at North Carolina State University was supported by the Office of Basic Energy Sciences, Division of Materials Sciences, U.S. Department of Energy, under Grant DE-FG05-86ER45259.

REFERENCES

1. J.-C. Bouloux and J. Galy, *Acta Crystallogr. B* **29,** 1335 (1973).
2. Y. Oka, T. Yao, N. Yamamoto, M. Ueda, and S. Maegawa, *J. Solid State Chem.* **149,** 414 (2000).
3. G. Liu and J. E. Greedan, *J. Solid State Chem.* **115,** 174 (1995).
4. Y. Zhang, C. J. Warren, R. C. Haushalter, A. Clearfield, D.-K. Seo, and M.-H. Whangbo, *Chem. Mater.* **10,** 1059 (1998).
5. S. Taniguchi, T. Nishikawa, Y. Yasui, Y. Kobayashi, M. Sato, T. Nishioka, M. Kontani, and K. Sano, *J. Phys. Soc. Jpn.* **64,** 2758 (1996).
6. R. Hoffmann, *J. Chem. Phys.* **39,** 1397 (1967).
7. K. Kodama, H. Harashina, H. Sasaki, Y. Kobayashi, M. Kasai, S. Taniguchi, Y. Yasui, M. Sato, K. Kakurai, T. Mori, and M. Nishi, *J. Phys. Soc. Jpn.* **66,** 793 (1997).
8. C. S. Hellberg, W. E. Pickett, L. L. Boyer, H. T. Stokes, and M. J. Mehl, *J. Phys. Soc. Jpn.* **68,** 3489 (1999).
9. M. A. Korotin, I. S. Elfimov, V. I. Anisimov, M. Troyer, and D. I. Khomskii, *Phys. Rev. Lett.* **83,** 1387 (1999).
10. K. S. Lee, H.-J. Koo, and M.-H. Whangbo, *Inorg. Chem.* **38,** 2199 (1999).
11. H.-J. Koo and M.-H. Whangbo, *Solid State Commun.* **111,** 353 (1999).

12. M.-H. Whangbo, H.-J. Koo, and K. S. Lee, *Solid State Commun.* **114,** 27 (2000).
13. H.-J. Koo and M.-H. Whangbo, *J. Solid State Chem.* **151,** 96 (2000).
14. E. Clementi and C. Roetti, *Atom. Data Nucl. Data Tables* **14,** 177 (1974).
15. P. J. Hay, J. C. Thibeault, and R. Hoffmann, *J. Am. Chem. Soc.* **97,** 4884 (1975).
16. O. Kahn and B. Briat, *J. Chem. Soc. Faraday II* **72,** 268 (1976).
17. O. Kahn, *Struct. Bond.* **68,** 89 (1987).
18. Our calculations were carried out by employing the CAESAR program package (J. Ren, W. Liang, and M.-H. Whangbo, "Crystal and Electronic Structure Analysis Using CAESAR." 1998. This book can be downloaded free of charge from the web site http://www.PrimeC.com/.)
19. O. Kahn, "Molecular Magnetism," VCH, Weinheim, 1993.